UAV-borne repeat-pass SAR interferometry and SAR tomography with a compact L-band SAR system

Othmar Frey
Gamma Remote Sensing, Gümligen, Switzerland / ETH Zurich, Switzerland
Email: frey@gamma-rs.ch / otfrey@ethz.ch

Charles L. Werner
Gamma Remote Sensing, Gümligen, Switzerland
Email: cw@gamma-rs.ch

Abstract

In this contribution, we present SAR image focusing, interferometric, and first tomographic processing results computed from repeat-pass SAR data sets acquired on-board of a vertical-take-off-and-landing (VTOL) unmanned aerial vehicle (UAV): the data was acquired using a novel compact FMCW L-band SAR system in two repeat-pass SAR campaigns flown on 2019-02-13 and 2019-03-28, respectively. In these demonstration campaigns, the Gamma L-band SAR system was deployed and operated on Aeroscout's VTOL UAV Scout B1-100. Repeat-pass interferograms and coherence maps with a temporal baseline of up to 43 days are presented and a tomographic profile obtained from short-term repeat-pass measurements is shown. The results demonstrate the feasibility of UAV-borne repeat-pass SAR interferometry and SAR tomography at L-band.

1 Introduction

In this contribution, we present SAR image focusing, interferometric, and first tomographic processing results obtained with repeat-pass SAR data sets acquired on-board of a vertical-take-off-and-landing (VTOL) unmanned aerial vehicle (UAV) system. The data was acquired using a novel compact frequency-modulated continuous-wave (FMCW) L-band SAR system in two repeat-pass SAR campaigns flown on 2019-02-13 and 2019-03-28, respectively. In these demonstration campaigns, the compact Gamma L-band SAR system was mounted on a Scout B1-100 UAV operated by Aeroscout. During the first campaign, the area was covered with snow, while during the second campaign most of the area except the higher mountains was snow-free. The test site includes different types of land cover including meadows, forest, rock, as well as a few man-made structures, such as buildings, fences, roads, a railroad, poles etc. This variety is useful to assess the level of coherence that can be obtained for the various landcovers at L-band. Repeat-pass interferograms and coherence maps with a temporal baseline of up to 43 days are presented and a vertical profile obtained from tomographic processing of 6 short-term repeat-pass SAR acquisitions is shown.

2 Methods and Data

2.1 L-band FMCW SAR System

The L-band radar features 4 low-noise receiver channels simultaneously, a custom-designed FPGA 14-bit/channel digitizer. The radar is controlled by a Linux computer. The transmitter switch (2 alternating transmit channels) permits full-pol data acquisitions, single-pass cross-track, along-track interferometric acquisitions and combination of these modes with up to 4 simultaneous receive channels. Total power consumption is less than 60W.

Frequency within	1.2 - 1.4 GHz
used center freq.	1.325 GHz
wavelength at center freq.	22.6 cm
Chirp bandwidth	50 - 200 MHz
used bandwidth	100 MHz
range res. (@ 100 MHz BW)	1.5 m
Azim. res. (@ full SA)	$\leq$ 0.5 m
Azim. res. (@ SA=250m, R=5km)	2.3 m
Type	FMCW
Chirp lengths	250 μs - 8 ms.
Transmit power	max. 10W (used: 5W)
Transmit channels	2 (alternating)
Receive channels	4 (simultaneous)
Elev. beamwidth (3dB)	40.0 deg
Azim. beamwidth (3dB)	40.0 deg
Elev. pointing angle	variable (config. dep.)
Radar hardware assembly	Pelicase 1450
Dimensions (l/w/h)	406/330/174 mm
Weight	7.65 kg

Table 1: Gamma L-band SAR specifications

2.2 SAR focusing, interferometric, and tomographic processing

The UAV-borne SAR data is focused using a time-domain back-projection (TDBP) approach [1] that we adapted for

(a) (b) (c)

Figure 1: The Gamma L-band SAR mounted on Aeroscout's UAV Scout B1-100 before take-off (a) in Feb. and (b) in Mar. 2019, and (c) during the repeat-pass multi-baseline SAR data acquisition in Wolfenschiessen, Switzerland, in March 2019. The compact radar hardware and the instrument computer are enclosed in the yellow pelicase. The two quadratic patch antennas (transmit and receive antennas) are mounted close to the Honeywell HGuide n580 INS/GNSS navigation system.

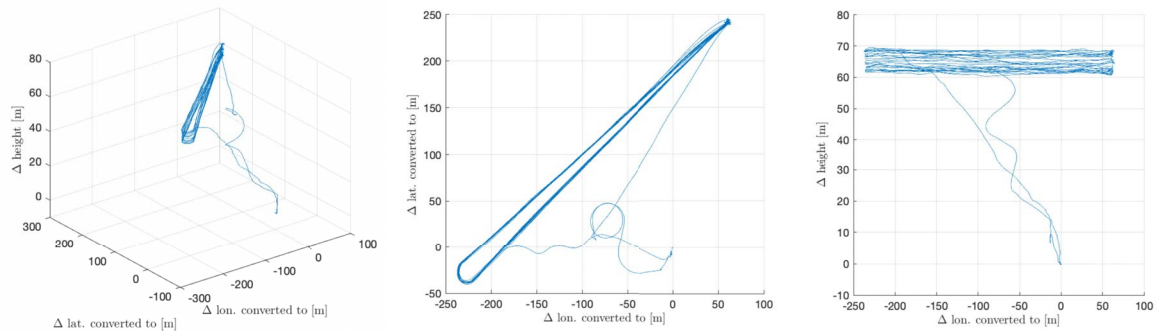

Figure 2: 3-D view of the complete UAV-borne SAR sensor trajectory (take-off to landing) of the second campaign on 20190328 (blue) as obtained from the on-board Honeywell HGuide n580 INS/GNSS system and a local GNSS reference station after post-processed kinematic (PPK) mode GNSS positioning and loosely-coupled fusion of the INS and GNSS data

FMCW SAR data processing [2, 3, 4] and that we implemented in C/CUDA [5] to run parallelized on an NVIDIA GPU. Our TDPB implementation considers the full 3-D geometry on a pulse by pulse basis therefore leading to well-focused imagery also for nonlinear sensor trajectories [1]. Likewise, the tomographic processing is obtained using the same TDBP approach the data being focused directly to a 3-D reconstruction grid in map coordinates as detailed in [6]. This approach allows for an approximation-free height-dependent calculation of the sample covariance matrix based on focused imagery at each layer.

2.3 Measurement setup / UAV flight trajectories

In Fig. 1, the Gamma L-Band FMCW SAR system mounted on Aeroscout's VTOL UAV Scout B1-100 is shown. Fig. 2 contains the UAV flight trajectories of the second repeat-pass campaign, in March 2019. The positioning and attitude of the SAR sensor is calculated as a post-processed kinematic (PPK) carrier-phase GNSS solution with respect to a local ad-hoc GNSS reference station in the field and then combined with the INS data (3-axis accelerations and angular velocities) in a loosely-coupled manner. The flight tracks of the two campaign days overlap partially providing a number of tracks with almost zero spatial baseline that can be exploited to calculate 43-day interferograms and coherence maps with minimal residual topographic phase and little volume decorrelation. Note, that only the trajectory of the second day is shown in Fig. 2 the repeat-pass acquisitions of which are used for the tomographic data processing. Their maximum vertical span is slightly less than 10 m.

3 Results

The main scene was covered with snow during the first campaign, whereas the lower part of the same scene was completely snow-free during the second campaign. This is expected to have a substantial impact on the 43-day coherence and interferometric phase for snow-covered / snow-free meadows. The forested areas consist of a mix of deciduous trees in leaf-off condition and evergreen coniferous trees. Fig 3 shows the repeat-pass interferometric results obtained for a short-term (5min) and a long-term (43-day) temporal baseline. Fig 4 shows a close-up view of a multi-look intensity image, and a zoomed view with a vertical tomographic transect obtained through multi-look beamforming tomographic focusing of the multi-baseline UAV-borne SAR data of the first campaign day.

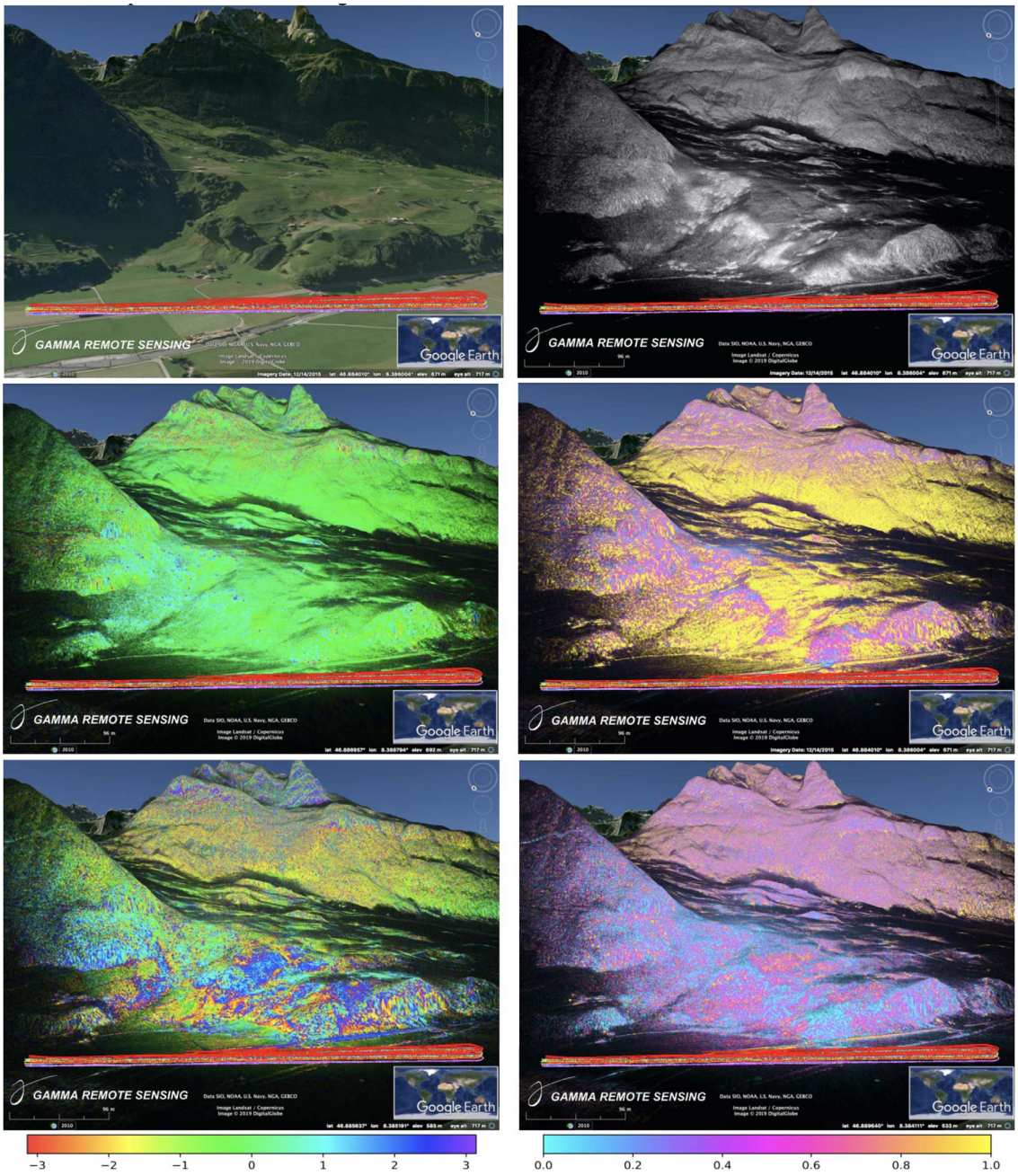

Figure 3: Top-left: scene overview, imaged side of the valley. Top right: SAR backscatter intensity image (20190328_095731). Middle: Short-term (5min) repeat-pass interferometric phase [rad] (left) and coherence (right) for the pair 20190328_095731_20190328_100237. Bottom: Long-term (43-days) interferometric phase (left) and coherence (right) for the pair 20190213_100832_20190328_101002. In the foreground, the flight trajectories are shown.

4 Discussion

Well focused SAR imagery was obtained for all tracks during both UAV-borne SAR campaigns on 2019-02-13 and 2019-03-28. Overlapping flight tracks (close to zero-baseline) were successfully flown during both campaigns by Aeroscout, so that coherent short term (pairs acquired in same campaign) and long-term (pairs acquired in campaigns separated by 43 days) interferograms could be generated.

Short-term interferograms: The Interferometric coherence is high for those pairs with small spatial baseline. The short-term interferometric phase is stable overall. In forested areas, phase changes due residual baselines and DEM/DSM (tree heights) lead to some phase changes. Depending on the view geometry (strong foreshortening/layover) and the remaining spatial baseline the interferometric phase is small on bare surfaces. Non-zero phases are visible in forested areas due to the scattering height difference relative to the DEM surface height. The stable phase of the short-term (5min) repeat-pass in-

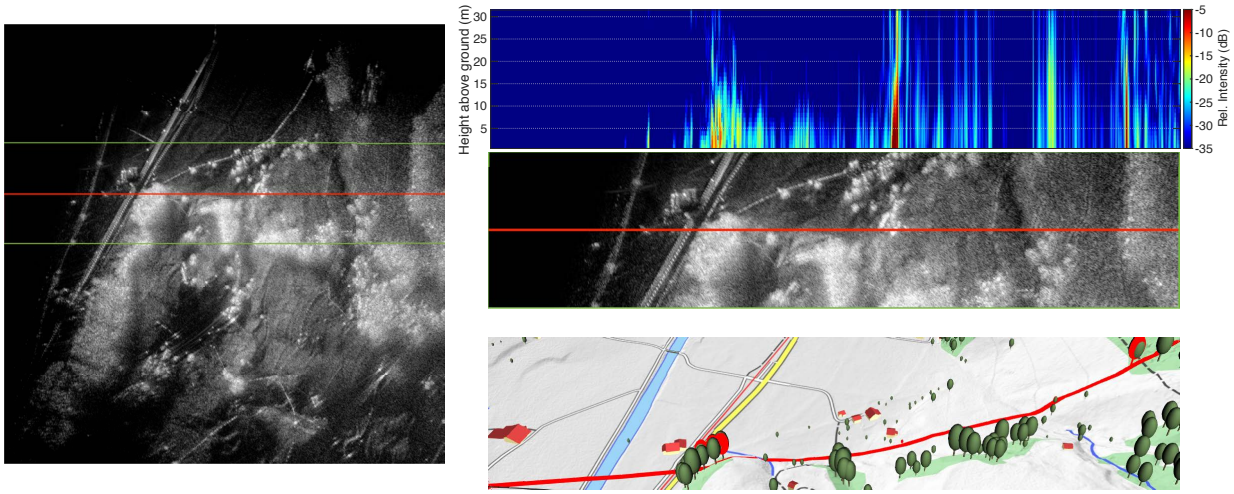

Figure 4: Left: SAR image focused onto a DEM in map coordinates (east./north.), hence called geoslc. Right: Zoomed view with the red line indicating the location of the west-east transect of the vertical tomographic slice shown above the SAR image. The colorbar indicates relative intensity in dB. Due to the high dynamic range the color scale is limited to a range of 30 dB (-5 to -35 dB) for visualization purposes. Bottom right: 3-D map rendering incl. 3-D objects for visual comparison; data ©swisstopo.

terferogram observed in the non-forested areas confirms that the SAR image focusing is of high quality and that also the positioning solution is of sufficient quality to obtain only very small residual unknown positioning errors compared to the wavelength at L-band. Such short-term interferograms with near-zero spatial baseline are therefore an adequate performance indicator that demonstrate the good quality of the entire repeat-pass interferometric system including the processing chain.

43-day long-term interferograms: Long-term interferometric phases can be successfully calculated for the long-term pairs with small spatial baselines. Long-term interferometric phase is altered by several aspects such as the snow/no-snow cover, changes in the vegetation, moisture, different gradients in the tropospheric layer etc. Long-term coherence is affected by several aspects: snow/ no-snow, slight changes in the vegetation, although the coherence stays in the mid-range for some of the forested areas, depending on the view geometry.

SAR Tomography: The tomographic slice shown in Fig. 4 was produced with 6 repeat-pass tracks to ensure appropriate baseline spacing. While the PPK and INS/GNSS-fused positioning accuracy is at cm level, real-time navigation of the UAV to the targeted flight tracks and operating within the desired flight tube (< 1m) remains challenging. The first ML beamforming results confirm a good tomographic focusing.

Conclusion/Outlook: Our results further confirm the feasibility of UAV-borne repeat-pass SAR interferometry and SAR tomography at L-band. Together with the car-borne setup of the Gamma L-band radar, as used for DInSAR-based mapping of surface displacements [7], these new agile SAR platforms are a promising and complementary means for (near-) terrestrial mobile mapping applications.

Acknowledgment

This research is carried out in the frame of a joint industry-academic research project supported by Innosuisse, P.-No. 18159.1. Many thanks to Aeroscout GmbH for the good cooperation and to J. Jang and Sang-Hoon Hong for supporting the UAV campaigns. A. Geiger and M. Meindl, ETH Zurich, are acknowledged for lending their Leica GNSS base station.

References

[1] O. Frey, C. Magnard, M. Rüegg, and E. Meier, "Focusing of airborne synthetic aperture radar data from highly nonlinear flight tracks," *IEEE Trans. Geosci. Remote Sens.*, vol. 47, no. 6, pp. 1844–1858, June 2009.

[2] A. Ribalta, "Time-domain reconstruction algorithms for FMCW-SAR," *IEEE Geosci. Remote Sens. Lett.*, vol. 8, no. 3, pp. 396–400, May 2011.

[3] C. Stringham and D. G. Long, "GPU processing for UAS-based LFM-CW stripmap SAR," *Photogrammetric Engineering & Remote Sensing*, vol. 80, no. 12, pp. 1107–1115, 2014.

[4] O. Frey, C. L. Werner, U. Wegmuller, A. Wiesmann, D. Henke, and C. Magnard, "A car-borne SAR and InSAR experiment," in *Proc. IEEE Int. Geosci. Remote Sens. Symp.*, 2013, pp. 93–96.

[5] O. Frey, C. L. Werner, and U. Wegmuller, "GPU-based parallelized time-domain back-projection processing for agile SAR platforms," in *Proc. IEEE Int. Geosci. Remote Sens. Symp.*, July 2014, pp. 1132–1135.

[6] O. Frey and E. Meier, "3-D time-domain SAR imaging of a forest using airborne multibaseline data at L- and P-bands," *IEEE Trans. Geosci. Remote Sens.*, vol. 49, no. 10, pp. 3660–3664, Oct. 2011.

[7] O. Frey, C. L. Werner, and R. Coscione, "Car-borne and UAV-borne mobile mapping of surface displacements with a compact repeat-pass interferometric SAR system at L-band," in *Proc. IEEE Int. Geosci. Remote Sens. Symp.*, 2019, pp. 274–277.